Lithuanian Journal of Physics, Vol. **58**, No. 1, pp. 99–107 (2018)

COMPACT DIFFRACTIVE OPTICS FOR THz IMAGING

L. Minkevičius, S. Indrišiūnas, R. Šniaukas, G. Račiukaitis, V. Janonis, V. Tamošiūnas,

I. Kašalynas, and G. Valušis

Center for Physical Sciences and Technology, Saulėtekio 3, 10257 Vilnius, Lithuania

Email: linas.minkevicius@ftmc.lt

Received 16 January 2018; accepted 22 March 2018

We present a compact diffractive silicon-based multilevel phase Fresnel lens (MPFL) with up to 50 mm in diameter and a numerical aperture up to 0.86 designed and fabricated for compact terahertz (THz) imaging systems. The laser direct writing technology based on a picosecond laser was used to fabricate diffractive optics on silicon with a different number of phase quantization levels *P* reaching an almost kinoform spherical surface needed for efficient THz beam focusing. Focusing performance was investigated by measuring Gaussian beam intensity distribution in the focal plane and along the optical axis of the lens. The beam waist and the focal depth for each MPFL were evaluated. The influence of the phase quantization number on the focused beam amplitude was estimated, and the power transmission efficiency reaching more than 90% was revealed. The THz imaging of less than 1 mm using a robust 50 mm diameter multilevel THz lens was achieved and demonstrated at 580 GHz frequency.

Keywords: binary optics, diffractive lenses, phase shift, three-dimensional fabrication, lenses, lens system design

PACS: 42.15.Eq, 42.79.Bh

1. Introduction

Suitability of terahertz (THz) imaging for nondestructive testing [1], biomedical research [2] or food and pharmaceutical industry [3] stimulates a search for compact and practically convenient solutions. It can be assumed that development of compact THz diffractive optics components, which enable massive parabolic mirrors to be replaced by much more attractive flat compact optical elements, is a particularly important issue [4, 5].

In this article, designs of multilevel phase Fresnel lenses (MPFLs), fabrication and focusing performance are studied. The design of MPFLs starts from P=2 phase quantization levels and extends up to a continuous kinoform shape. Samples were developed for the focusing of 580 GHz frequency radiation.

2. Samples and fabrication

Silicon wafer of 0.46 mm thickness was patterned using an industrial-scale-compatible laser direct writing (LDW) system based on a 1064 nm wavelength, 13 ps pulse duration, 1 MHz repetition rate, 60 μJ peak energy laser (Atlantic 60 from *Ekspla Ltd.*) [6]. The LDW technology enabled us to manufacture different complexity multilevel zone-phase elements in the same process with the opportunity to modify parameters in time.

Two groups of the MPFL samples with an outside diameter of 17.5 mm and the focal distances of 10 and 5 mm and one sample with a 50 mm diameter and a focal distance of 30 mm were designed and fabricated. The group of the 17.5 mm diameter MPFL contained five samples with a different number of phase quantization levels for each focal

distance allowing to figure out the optimal phase quantization level [5]. Radii and depths of the subzones were calculated according to the methodology presented in [7].

The SEM images of the 5 mm focal length MPFL with 4 subzones are shown in Fig. 1(a, b). The step-profile scanned across the centre of each sample is given in Fig. 1(c). The photo of the flat 50 mm diameter MPFL with $P = 16$ quantization levels is depicted in Fig. 1(d). As one can see, a step-like structure of individual zones starts to merge into a continuous kinoform shape for the case of 8 phase quantization levels. Such transition from a step-like to a kinoform shape occurred due to the limited size of an ablation spot of approximately 44 μm. Fig. 1(b) shows the SEM picture of the surface microstructure at each area of 4-step MPFL. The laser-processed surface of silicon contained randomly distributed columnar structures the average size of which was increasing with longer exposure by the laser. Such an increase of surface roughness and the growth of columnar morphology with a number of laser pulses were well-known phenomena in materials laser processing [8, 9]. When the first layers in materials were ablated, nanostructures were randomly formed inside the ablated area due to hydrodynamical processes involved. Then, with an each following laser exposure, nanoscaled features grow and merge into micrometre-scale self-organized conical structures. In our earlier study [10], it was noticed that the laser ablation of silicon affected terahertz properties of a material even though the roughness of the processed area was much smaller than the wavelength.

3. Results and discussion

The focusing performance of the multilevel phase Fresnel lens was investigated by measuring Gaussian

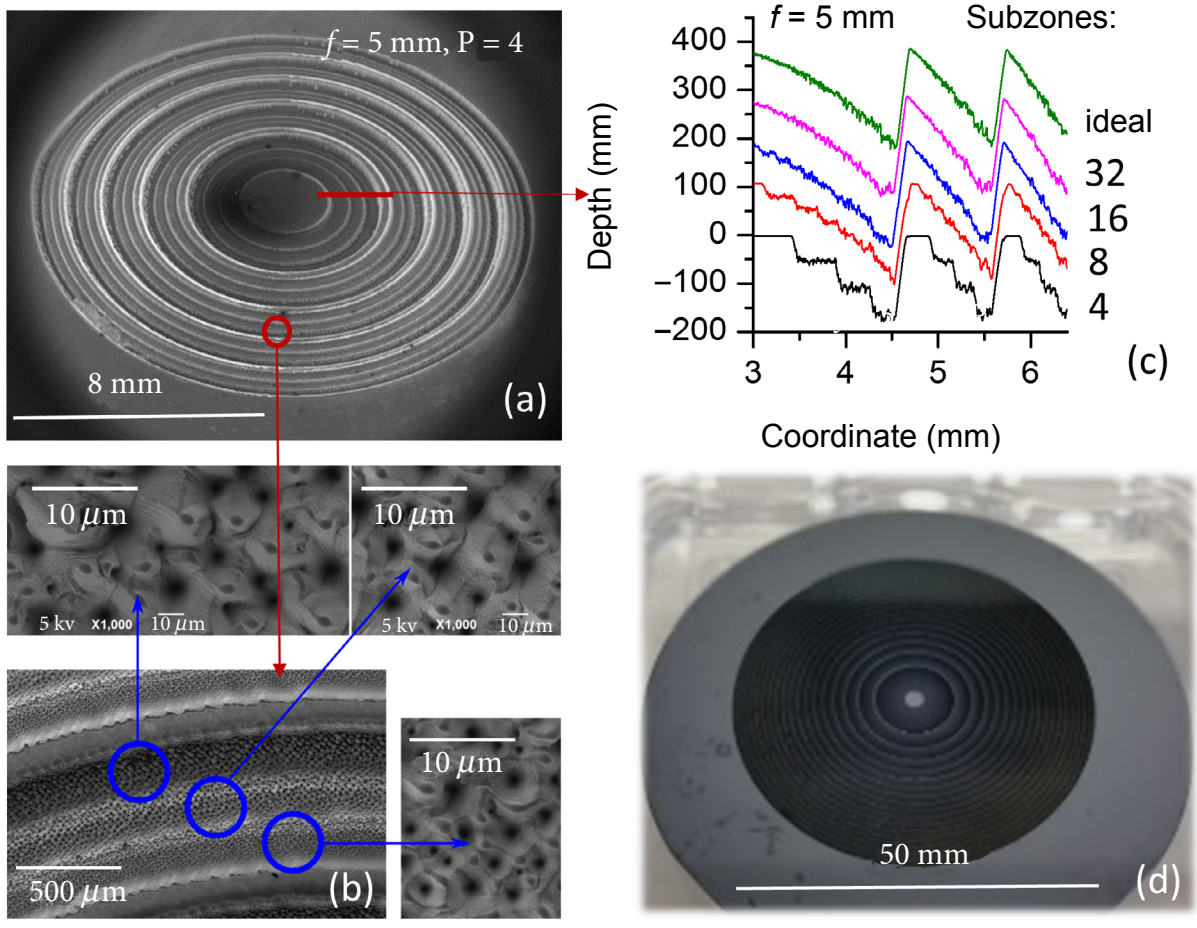

Fig. 1. The SEM image of the MPFL with the focal distance $f = 5$ mm consisting of 4 phase quantization levels (a), the zoomed area of each subzone (b). The cross section of the 5 mm focal length MPFL measured with a step profiler (c). Each following profile line was moved by 100 μm [5]. The photo of the 50 mm diameter, 16 subzones MPFL with the focal length $f = 30$ mm (d).

beam intensity distribution in the focal plane and along the optical axis at 0.58 THz frequency. The experiment was performed using the *Virginia Diodes* multiplier chain VDI MC156 as a THz radiation source. Radiation was collimated by a 12 cm focal length high density polyethylene (HDPE) lens and, using a 50 mm diameter mirror, it was guided to the MPFL under investigation. Focused radiation was registered with a resonant THz antenna-coupled micro-bolometer detector [11]. The intensity distribution in the focal plane and the focal depth in the case of MPFL with f = 30 mm, f = 10 mm and f = 5 mm is shown in Fig. 2. The estimated beam waist for the 50 mm diameter MPFL reaches 0.92 mm, and the focal depth is 4.27 mm, respectively. The focusing was found to be sharper using the f = 5 mm in comparison with the f = 10 mm MPFL, while peak intensities were evaluated to be similar. Noticeable asymmetrical Airy disks could be caused by lens misalignment and gradient of the subzone height formed during fabrication. The shadowing effect, which is well known in binary gratings with deep grooves [12], was also considered. In order to investigate this effect, geometrical calculations were performed. Red (online) lines in Fig. 2(a, b) indicate how the 5 and 10 mm focal length MPFL outer zones "see" the focal spot. With our lens design, three favourable factors are expected to play a significant role. Firstly, vertical walls obstructing paths of secondary waves are

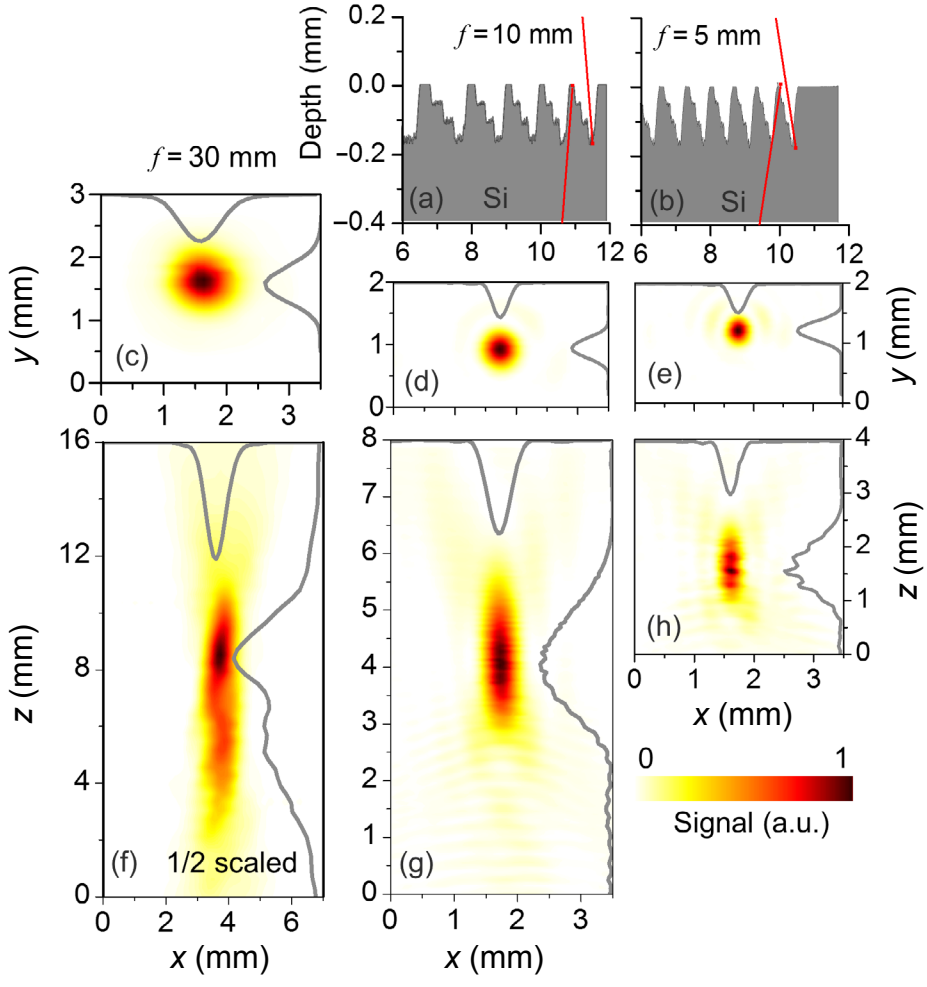

Fig. 2. Experimental 2D beam profiles of the investigated MPFL with focal length f = 30 mm, f = 10 mm [5] and f = 5 mm [5] in the focal plane (*xy* direction) (c–e) and in the focal depth (*xz* direction) (f–h). Geometrical red (online) lines indicate how the 10 and 5 mm focal length MPFL outer zones "see" the focal spot (a, b). The beam cross sections at maximum intensity are presented in a linear scale as a solid line for each case.

simply not present in the case of kinoform lenses, once the structured surface faces the focal point. As can be seen, in Fig. 2(a, b) minor shadowing may be expected in the case of 5 mm focal length lenses, but with an increase of the number of subzones the steep part of the zone causing shadowing diminishes. Shadowing may cause some decrease of efficiency with zone plates having less than 4 subzones, however, other effects also should be taken into account. Once the flat surface faces the focal point, a relatively large refractive index of silicon ($n = 3.48$) minimizes the angles of incidence within Si due to Snell's law and shadowing. Furthermore, nominally vertical walls are not perfectly vertical due to laser processing, as seen in Fig. 1(c).

The peak signal dependence on the phase quantization number for the 5 and 10 mm focal length MPFLs is shown in Fig. 3. It is clearly seen that the peak signal saturates at 8 phase quantization levels. This result is in a good agreement with theoretical diffraction efficiency distribution [13]. A detailed investigation was performed aiming to explain the signal deviation in the case of 16 and >1000 phase quantization levels.

Diffraction efficiency was evaluated by integrating the THz beam intensity measured at the focal *xy* plane and accounting the absorption losses of silicon before and after laser ablation. The results are presented in Table 1. As was shown in Fig. 3, MPFLs with $P > 8$ exhibited high diffraction efficiency values. Lower efficiency was observed for the MPFL with $f = 5$ mm due to a higher power dissipation in the secondary lobes of diffraction maxima (Fig. 2(d)). The absolute value of focused beam intensity was found to be dependent on the THz reflection and absorption losses in the laser affected silicon (Fig. 4). It is worth noting that laser ablation changes silicon transmittance due to the following reasons. The first one is re-solidified material on the silicon surface [14, 15]. This layer absorbs THz radiation, and the greater the ablated area, the stronger THz radiation absorption is observed. The second reason concerns the roughness of the ablated silicon: THz transmittance from these modified areas is reduced by about 49% in comparison to those that are unmodified (Fig. 4) because of the enhancement of absorption of black silicon [10]. It is also important to note that different percentage of the laser ablated surface, as in $P = 32$ MPFL, has a notable unaffected zone in the centre, while in the kinoform MPFL it is not pronounced, as it can be seen in Fig. 1. Moreover, a closer inspection of the zone structure has revealed that every zone in the kinoform MPFL differs from $P = 32$ MPFL, as below the 100 μm depth less material has been ablated. This change in the form of the zone diminishes the focusing efficiency. The origin of this distortion may be attributed to a flaw in the fabrication process. That is why the efficiency in the case of the 5 mm focal length kinoformly shaped MPFL is slightly smaller than the MPFL with 32 phase quantization levels.

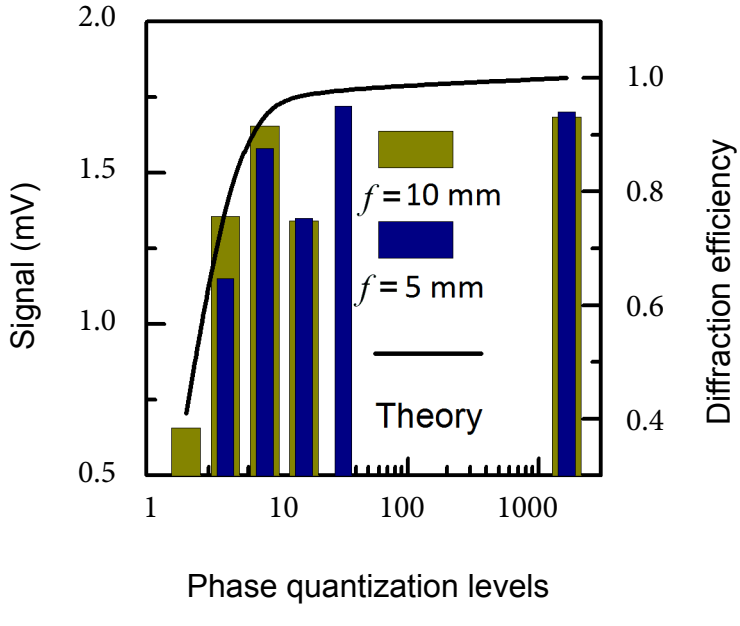

Fig. 3. Peak signal of the THz detector dependence on the phase quantization number *P*. Theory is diffractive efficiency of the Si-lens depending on the number of phase quantization levels [5].

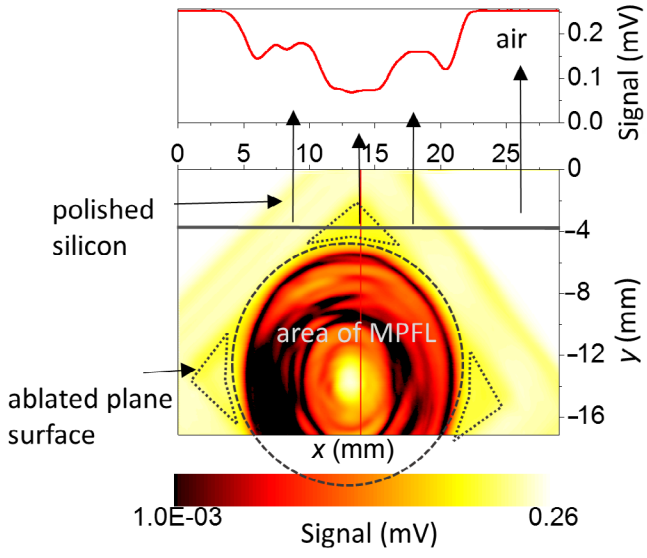

Fig. 4. Silicon transmittance at 0.58 THz through differently affected surfaces of MPFL. Note the 2D transmission image is plotted in a logarithmic scale.

The change of focused beam intensity distribution and the full width at half maximum (FWHM) of the Gaussian beam along an optical z axis is shown in Fig. 5. The results are presented for two cases: the zone plate surface is faced to a detector (blue online) and to an emitter (dark yellow online). The focusing parameters like the beam waist and the focal depth for each MPFLs are presented in Table 1. As can be noticed in Fig. 5, the interference fringes are more pronounced in the case when the MPFL plane is orientated to the detector. This effect can be ascribed to the formation of standing cavity waves between the diffractive lens and the THz detector without antireflection coating. The ablated silicon plane scatters the incident radiation back, instead of normal reflection. Proper orientation of the MPFL allows us to get a focused terahertz beam without a change in the FWHM value and signal rippling.

The comparison of 580 GHz beam cross-sections focused with different diffractive optics designs is presented in Fig. 6. As can be seen, the lenses with numerical aperture NA = 0.86 perform very

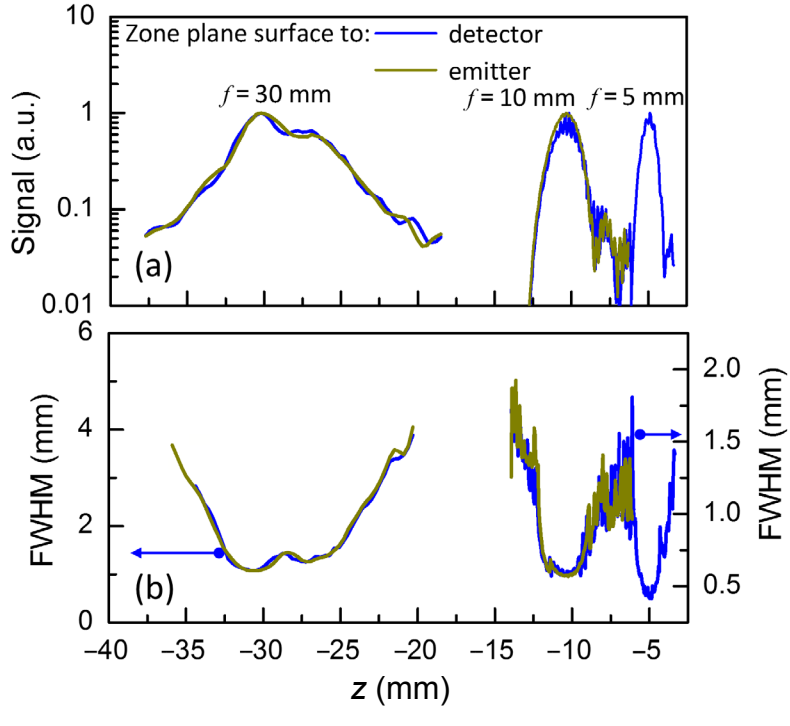

Fig. 5. Focused beam intensity (a) and FWHM (b) value change along the z coordinate for the case of kinoform MPFL with f = 5 and 10 mm [5] and 50 mm diameter MPFL. The laser-ablated silicon surface was facing the THz detector or the emitter as indicated.

Table 1. The design parameters and performance of the developed MPFL. Here f is the focal length; NA is the numerical aperture; P is the number of subzones; ω_0 is the beam waist; b is the distance between two axial points at which the beam waist increased by a value of $\sqrt{2}$, i.e. focal depth; E_F is the focusing efficiency (ratio between the integrated detector signal in cases of a focused beam and an unfocused beam).

f, mm	NA	P	Subzone height, μm	ω_0, mm	b, mm	E_F, %
10	0.65	2	139	0.45	2.84	27
		4	56	0.44	2.46	58
		8	25	0.48	3.7	71
		16	13	0.49	3.44	56
		kinoform	0.9	0.48	2.62	72
5	0.86	4	56	0.39	1.42	41
		8	27	0.35	1.18	55
		16	15	0.37	1.32	51
		32	8	0.36	1.14	66
		kinoform	0.9	0.35	1.04	65
30	0.64	16	15	0.92	4.27	93

similarly and independently of fabrication technology and used material. In the case of the 10 mm focal length MPFL, a wider FWHM reaching 0.42 mm is observed. The case with the 50 mm diameter MPFL has shown about 2 times wider FWHM value. However, amplitudes of the detector signal could not be compared due to different experiment conditions. The measured absolute diffraction efficiency for silicon MPFLs is presented in Table 1.

The comparison of the metal zone plate and commercial parabolic mirror focusing performance was presented in [4]. It was shown that the imaging system with the 5 mm focal length zone plate improves the spatial resolution up to 25% in comparison with that of a commercial parabolic mirror. Using the same experimental set up, presented in [4], the resolution target imaging using the 50 mm diameter THz MPFL is recorded. The imaging result of the resolution target and the plastic card containing an USB stick is shown in Fig. 7. As one can see, periodic stripes were distinguishable if the period was not smaller than 1 mm (Fig. 7(b)). Such result is comparable with the parabolic mirror performance, but it has an advantage of a compact size and absence of Fabry–Perrot oscillations, as observed in the case with a metal zone

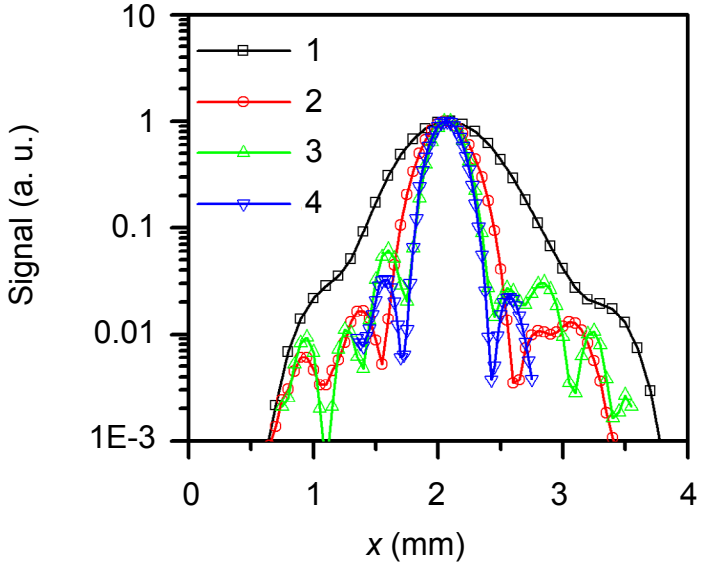

Fig. 6. Cross-section of the 580 GHz beam focused with different designs of zone plates in the focal plane of diffractive optics. 1 is P = 16, f = 30 mm, d = 50 mm MPFL; 2 is P = 16, f = 10 mm, d = 17 mm MPFL; 3 is P = 16, f = 5 mm, d = 17 mm MPFL [5]; 4 is P = 1, f = 5 mm, d = 17 mm metal zone plate [18]. P, the phase quantization level; f, the focal distance; d, the diameter.

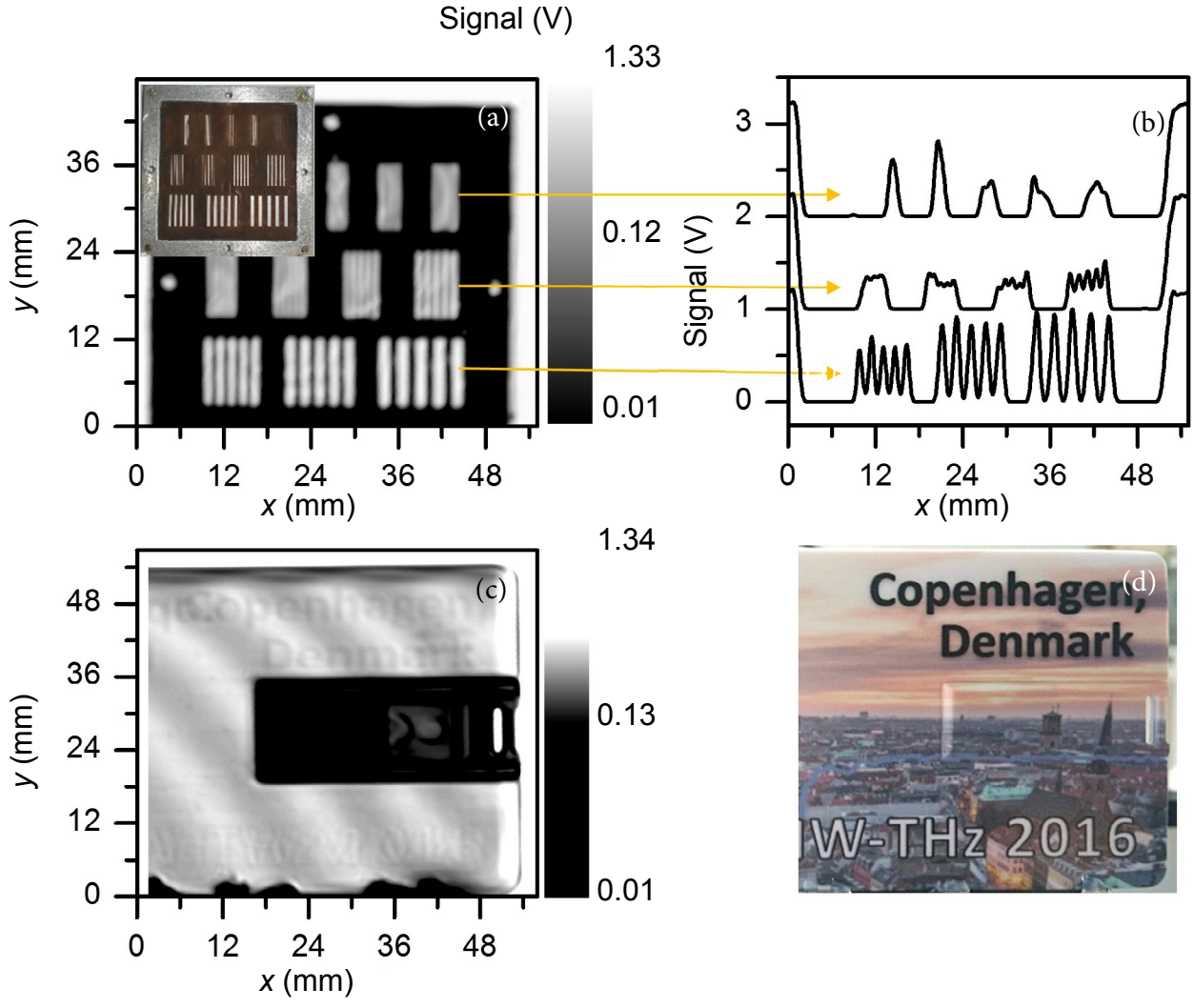

Fig. 7. The THz image of the resolution target at 580 GHz frequency obtained by a 3 cm focal length diffractive lens (a). The pixel size 0.1 × 0.1 mm^2. The image consists of 590 × 493 pixels. Dark colour in the THz images corresponds to the transmittance minimum. The cross-section of the resolution target, stripes with different periods (b). The vertical scale is shifted by 1 V. The photo of the resolution target is shown in the inset of (a). Detailed target parameters are described in [4]. The THz image of the plastic card containing a USB stick (c). The pixel size 0.1 × 0.1 mm^2. The image consists of 590 × 568 pixels. The photo of the plastic card (d).

plate [16, 17]. The 580 GHz image of a plastic card reveals the structure of internal components like an integrated circuit and letters due to a different transmittance of THz radiation. The standing waves are observed in a plastic structure with smooth and nearly parallel surfaces due to constructive wave reflections between a sample and a detector plane.

4. Conclusions

The laser direct writing technology was found to be both powerful and convenient tool to fabricate diffractive optics for THz frequencies. The multilevel phase Fresnel lenses for 580 GHz reaching 0.86 numerical apertures have been fabricated with a different number of phase quantization levels. The effect of the phase quantization number on the focused beam amplitude was determined, and the transmittance reaching more than 90% was demonstrated. It was shown that the imaging resolution of less than 1 mm can be obtained employing a robust 50 mm diameter multilevel THz lens at 580 GHz frequency.

Acknowledgements

This work was supported by the Research Council of Lithuania (LAT 04/2016).

References

[1] P. Lopato, G. Psuj, and B. Szymanik, Non-destructive inspection of thin basalt fiber reinforced composites using combined terahertz imaging and infrared thermography, Adv. Mater. Sci. Eng. **2016**, 1–13 (2016).

[2] K.W. Kim, K.-S. Kim, H. Kim, S.H. Lee, J.-H. Park, J.-H. Han, S.-H. Seok, J. Park, Y. Choi, Y.Il Kim, J.K. Han, and J.-H. Son, Terahertz dynamic imaging of skin drug absorption, Opt. Express **20**(9), 9476–9484 (2012).

[3] J.A. Zeitler, P.F. Taday, D.A. Newnham, M. Pepper, K.C. Gordon, and T. Rades, Terahertz pulsed spectroscopy and imaging in the pharmaceutical setting – a review, J. Pharm. Pharmacol. **59**(2), 209–223 (2007).

[4] I. Kašalynas, R. Venckevičius, L. Minkevičius, A. Sešek, F. Wahaia, V. Tamošiūnas, B. Voisiat, D. Seliuta, G. Valušis, A. Švigelj, and J. Trontelj, Spectroscopic terahertz imaging at room temperature employing microbolometer terahertz sensors and its application to the study of carcinoma tissues, Sensors **16**(4), 432 (2016).

[5] L. Minkevičius, S. Indrišiūnas, R. Šniaukas, B. Voisiat, V. Janonis, V. Tamošiūnas, I. Kašalynas, G. Račiukaitis, and G. Valušis, Terahertz multilevel phase Fresnel lenses fabricated by laser patterning of silicon, Opt. Lett. **42**(10), 1875 (2017).

[6] B. Voisiat, S. Indrišiūnas, R. Šniaukas, L. Minkevičius, I. Kašalynas, and G. Račiukaitis, Laser processing for precise fabrication of the THz optics, Proc. SPIE **10091**, 100910F (2017).

[7] W.G.J.M. Rodríguez and H.D. Hristov, in: *41st European Microwave Conference* (IEEE, Manchester, 2011) pp. 894–897.

[8] J. Zhu, G. Yin, M. Zhao, D. Chen, and L. Zhao, Evolution of silicon surface microstructures by picosecond and femtosecond laser irradiations, Appl. Surf. Sci. **245**(1), 102–108 (2005).

[9] C.A. Zuhlke, T.P. Anderson, and D.R. Alexander, Formation of multiscale surface structures on nickel via above surface growth and below surface growth mechanisms using femtosecond laser pulses, Opt. Express **21**(7), 8460 (2013).

[10] I. Kašalynas, R. Venckevičius, L. Tumonis, B. Voisiat, D. Seliuta, G. Valušis, and G. Račiukaitis, Reflective terahertz imaging with the TEM_{01} mode laser beam, Appl. Opt. **52**(23), 5640 (2013).

[11] J. Trontelj, G. Valušis, R. Venckevičius, I. Kašalynas, A. Sešek, and A. Švigelj, A high performance room temperature THz sensor, Proc. SPIE **199**, 91990K (2014).

[12] Y. Zhang, C. Zheng, and Y. Zhuang, Effect of the shadowing in high-numerical-aperture binary phase Fresnel zone plates, Opt. Commun. **317**, 88–92 (2014).

[13] E.D. Walsby, S. Wang, J. Xu, T. Yuan, R. Blaikie, S.M. Durbin, X.-C. Zhang, and D.R.S. Cumming, Multilevel silicon diffractive optics for terahertz waves, J. Vac. Sci. Technol. B **20**(6), 2780 (2002).

[14] S. Indrišiūnas, B. Voisiat, A. Rėza, I. Šimkienė, R. Mažeikienė, A. Selskis, and G. Račiukaitis, Effect of laser-induced conversion of silicon nitride to silicon oxy-nitride on antireflective properties of passivation layer in polysilicon solar cells, Opt. Mater. Express **5**(7), 1532 (2015).

[15] M.E. Shaheen, J.E. Gagnon, and B.J. Fryer, Femtosecond laser ablation behavior of gold, crystalline silicon, and fused silica: a comparative study, Laser Phys. **24**(10), 106102 (2014).

[16] L. Minkevičius, B. Voisiat, A. Mekys, R. Venckevičius, I. Kašalynas, D. Seliuta, G. Valušis, G. Račiukaitis, and V. Tamošiūnas, Terahertz zone plates with integrated laser-ablated bandpass filters, Electron. Lett. **49**(1), 49–50 (2013).

[17] L. Minkevičius, K. Madeikis, B. Voisiat, I. Kašalynas, R. Venckevičius, G. Račiukaitis, V. Tamošiūnas, and G. Valušis, Focusing performance of terahertz zone plates with integrated cross-shape apertures, J. Infrared Millim. Terahertz Waves **35**(9), 699–702 (2014).

[18] L. Minkevičius, V. Tamošiūnas, I. Kašalynas, R. Venckevičius, K. Madeikis, B. Voisiat, D. Seliuta, G. Račiukaitis, and G. Valušis, On-chip integration solutions of compact optics and detectors in room-temperature terahertz imaging systems, Proc. SPIE **9585**, 95850M (2015).

KOMPAKTINĖ DIFRAKCINĖ OPTIKA TERAHERCŲ VAIZDINIMO SISTEMOMS

L. Minkevičius, S. Indrišiūnas, R. Šniaukas, G. Račiukaitis, V. Janonis, V. Tamošiūnas, I. Kašalynas, G. Valušis

Fizinių ir technologijos mokslų centras, Vilnius, Lietuva

Santrauka

Darbe pristatomi kompaktiški silicyje suformuoti difrakciniai Frenelio lęšiai, skirti terahercinio dažnio (THz) vaizdinimo sistemoms. Jie pagaminti naudojant lazerinės abliacijos technologiją. Šiuo metodu silicio paviršiuje suformuota 5 ir 10 mm židinio nuotolio difrakcinė zoninė plokštelė su skirtingais fazinio kvantavimo lygiais pasiekiant beveik tolygų sferinį paviršių, reikalingą efektyviam THz spinduliuotės fokusavimui. Šių lęšių skersmuo siekia iki 50 mm, o skaitinė apertūra neviršija 0,86 mm. Fokusavimo efektyvumas ištirtas matuojant Gauso pluošto intensyvumo pasiskirstymą židinio plokštumoje ir optinės ašies kryptimi. Įvertintas sufokusuoto Gauso pluošto sąsmaukos plotis ir kiekvienos Frenelio lęšio konfigūracijos židinio gylis. Išmatavus fazinio kvantavimo skaičiaus įtaką fokusuotos spinduliuotės amplitudei nustatyta, kad 8 pazonių difrakcinio lęšio fokusavimo efektyvumas sotinasi, kai pralaidumo koeficientas pasiekia daugiau nei 90 %. Atlikti THz vaizdinimo eksperimentai parodė, kad naudojant tvirtą 50 mm Frenelio lęšį galima pasiekti geresnę nei 1 mm skyrą ties 580 GHz dažniu.